

A Quantum Generative Framework for Modeling Single-Cell Transcriptomes with Gene-Gene and Cell-Cell Interactions

Selim Romero^{1,2,3*}, Vignesh Kumar¹, Robert S. Chapkin^{2,3},
James J. Cai^{1,3,4*}

¹Department of Veterinary Integrative Biosciences, Texas A&M University, 400 Bizzell St, College Station, 77843, TX, USA.

²Department of Nutrition, Texas A&M University, 400 Bizzell St, College Station, 77843, TX, USA.

³CPRIT Single Cell Data Science Core, Texas A&M University, 400 Bizzell St, College Station, 77843, TX, USA.

⁴Department of Electrical and Computer Engineering, Texas A&M University, 400 Bizzell St, College Station, 77843, TX, USA.

*Corresponding author(s). E-mail(s): ssromerogon@tamu.edu;
jcai@tamu.edu;

Contributing authors: vignesh_sk@tamu.edu; r-chapkin@tamu.edu;

Abstract

Single-cell RNA sequencing (scRNA-seq) data simulation is limited by classical methods that rely on linear correlations, failing to capture the intrinsic, nonlinear dependencies and the simultaneous gene-gene and cell-cell interactions. We introduce qSimCells, a novel hybrid quantum-classical simulator that leverages quantum entanglement to model single-cell transcriptomes. The core innovation is a quantum kernel that uses a parameterized quantum circuit with CNOT gates to encode complex, nonlinear gene regulatory network (GRN) and cell-cell communication topologies with explicit directionality (causality). The synthetic data exhibits non-classical dependencies that challenge standard analysis. We demonstrated that classical correlation methods (Pearson and Spearman) failed to reconstruct the complete programmed quantum causal paths, instead reporting spurious statistical artifacts driven by high base-gene expression probabilities. Applying CellChat2.0 to the simulated cell-cell communication validated the true

mechanistic links by showing a robust, relative increase in communication probability (up to 75-fold) only when the quantum entanglement was active. This work confirms that the quantum kernel is essential for creating high-fidelity ground truth data, highlighting the need for advanced inference techniques to capture the complex, non-classical dependencies inherent in gene regulation.

Keywords: Quantum Computing, Quantum Sampler, Biophysics, Bioinformatics, Single-cell

1 Introduction

Single-cell RNA sequencing (scRNA-seq) has revolutionized our understanding of biology by providing a snapshot of gene expression within individual cells[1]. This capability allows us to explore the unique molecular signatures that define a cell’s identity and function, a phenomenon known as cellular heterogeneity. Gene expression isn’t a simple, linear process; it’s a complex dance of interacting genes that form intricate gene regulatory networks (GRNs) which are fundamental to a cell’s proper function[2].

Simulating single-cell data is instrumental for computational approaches aimed at understanding cellular heterogeneity. Existing simulators, such as SERGIO and scMultiSim, have made significant strides in providing a controlled environment for benchmarking new computational tools[3, 4]. SERGIO, for instance, models gene expression dynamics and stochasticity using a user-provided GRN and differential equations[3]. scMultiSim expands on this by generating multimodal data, including scRNA-seq, chromatin accessibility, and spatial locations, to model a broader range of biological factors simultaneously[4]. Despite advancements, classical simulators rely on simplifying assumptions about underlying distributions and relationships, often failing to capture the intricate, nonlinear dependencies inherent in biological systems [5, 6]. Most importantly, they lack the capacity to simulate the simultaneous interplay between genes and cells. Existing methods typically approximate complex interactions using approaches rooted in linear correlations—a fundamental limitation of classical computing. We previously demonstrated a quantum framework for inferring Gene Regulatory Networks (GRNs) from single-cell RNA sequencing (scRNA-seq) data, known as quantum single-cell GRN (qscGRN). This approach is based on a parameterized quantum circuit designed to use qubit entanglement to simulate interactions between genes. The optimization was achieved using a quantum-classical framework that minimizes a loss function based on Kullback-Leibler (KL) divergence. This methodology exploits the potential of quantum computing to unravel complex single-cell GRNs beyond the limits of conventional statistical methods such as correlation and regression[7].

Our work introduces a novel hybrid quantum-classical simulator that addresses these limitations by leveraging the unique capabilities of quantum computers: superposition and entanglement. In our approach, qubits are used as an analogue for genes or features. We begin by applying custom rotation gates to each qubit, which acts

as an initial activator similar to a gene's basal expression level. We then use CNOT gates to create entangled relationships between selected qubits, directly modeling the nonlinear topology of a GRN. This approach enables the simulation of a richer and more diverse range of gene expression patterns than classical methods can achieve [7]. Furthermore, by entangling ligand and receptor genes, we are able to model cell-cell interactions and capture the cross-talk that occurs between multiple cell types.

Thus, the key focus of our work is to simulated intra-cellular communication and its relationship with inter-cellular signals. We explicitly model distinct gene sets from two different cell types using quantum circuit including: internal GRNs for each cell type, where one cell type has the ligand and the other cell type contains the receptor. This enables a more direct and robust simulation of cell-cell communication than is typically inferred by local neighborhood analysis in classical simulators.

2 Methods

Our present work was inspired by previous methods to generate scRNA-seq synthetic data, where methods relied on differential equations for stochastic interaction within genes to modulate cells and neighborhood interaction[3, 8]. In this work, we propose a different approach to generate synthetic scRNA-seq data as shown in Fig. 1. The main component of the single-cell generator is the quantum kernel, which empowers non-classical interactions through a rich quantum entangled GRN and feature entangled by LR pairs across different statevectors[7].

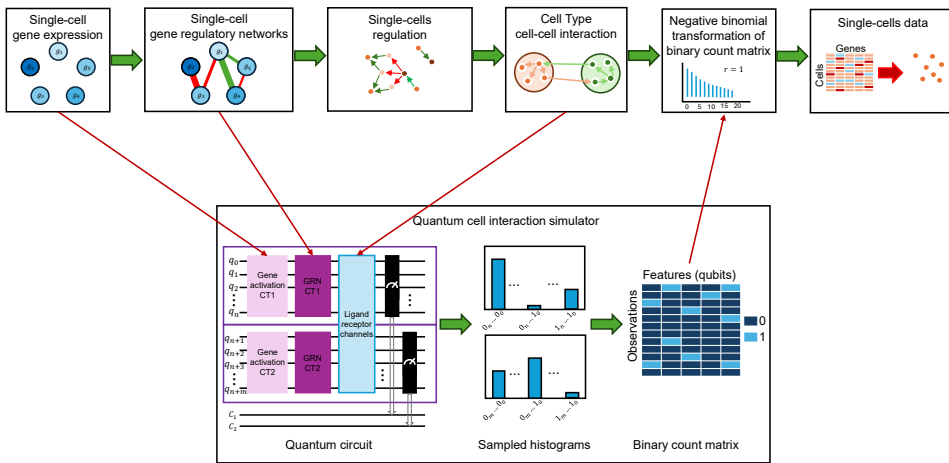


Fig. 1 Quantum single-cell data simulation.

2.1 Quantum kernel of qSimCells

Quantum computing offers a very interesting perspective for modeling relationships within genes and between cell types[7]. Our proposition utilizes a Parameterized Quantum Circuit (PQC) where the initial cell state $|\psi_0\rangle$ is prepared using user-defined gene activation angles θ_i .

The state initialization involves applying Y -axis rotation (R_y) to each of the n qubits, which starts in the ground state $|0\rangle$:

$$|\psi_0\rangle = \otimes_{i=0}^{n-1} R_y(\theta_i) |0_i\rangle. \quad (1)$$

Next, to integrate GRN interactions, we couple the expression of one gene to another using the Controlled-NOT (CX) gates. This process provides a unique entanglement inaccessible to classical computing, effectively pairing gene expressions to enforce activation or deactivation by a given gene (qubit)[7].

The resulting entangled state $|\psi_1\rangle$ is obtained by applying a sequence of M CX gates, where the sequence is crucial due to the non-commuting nature of the gates, potentially mimicking cascade activations:

$$|\psi_1\rangle = \left(\prod_{k=0}^{M-1} CX_{c_k, t_k} \right)_{\text{time-ordered}} |\psi_0\rangle. \quad (2)$$

The time ordered product means that the gates are applied sequentially, with CX_{c_1, t_1} applied first and $CX_{c_{M-1}, t_{M-1}}$ applied last. The sequence of CX gates is explicitly defined by the list of control-target pairs $L = \{(c_k, t_k)\}_{k=0}^{M-1}$, which represents the GRN topology[7].

A key advantage of quantum computing lies in its ability to combine states via the tensor product, which drastically expands the Hilbert space and enables complex interactions[9]. We can prepare two independent cell states, $|\psi_1\rangle$ (on n qubits) and $|\psi'_1\rangle$ (on n' qubits), which are initially defined on disjoint sets of qubits. The combined state is formed by their tensor product:

$$|\psi_2\rangle = |\psi_1\rangle \otimes |\psi'_1\rangle. \quad (3)$$

The resulting composite state $|\psi_2\rangle$ lives in a Hilbert space of dimensions $2^{n+n'}$ and serves as the foundation for modeling inter-state interactions (e.g., between different cell types) by applying subsequent entangling gates across the n and n' qubit registers, similar to the coupling defined in Eq. 2[9]. Crucially, we kept the measurements for the two different cell state registers separated, allowing for independent analysis.

2.2 Final entanglement and quantum simulation

To complete the model, we apply a final set of entangling gates across the combined $|\psi_2\rangle$ state to model **inter-state interactions** (e.g., cell-to-cell communication between the n and n' gene registers). This is achieved by applying a fixed sequence of K CX gates. The resulting final state, $|\psi_{\text{final}}\rangle$, is defined as:

$$|\psi_{\text{final}}\rangle = \left(\prod_{k=0}^{K-1} \text{CX}_{c'_k, t'_k} \right)_{\text{time-ordered}} |\psi_2\rangle. \quad (4)$$

The indices c'_k and t'_k here represent global qubit indices that span both the n and n' registers. The $|\psi_{\text{final}}\rangle$ state is obtained and executed using the Qiskit quantum computing framework developed by IBM[10]. Our methodology supports two implementations: for model demonstration, the circuit is run on the local quantum computer simulator, the AerSimulator; for realistic results incorporating quantum hardware noise, the circuit is executed on an IBM Quantum computer[10]. In both cases, the probability distribution of the final state is sampled by executing a fixed number of measurement shots using the SamplerV2 primitive. The number of shots, N_{shots} is set equal to the total number of simulated single-cell observations m . Furthermore, the raw output bit strings from the simulation are reversed (e.g., $b = b_{n-1}...b_0$) to align with the logical gene indices $i = 0 \dots n-1$, compensating for the little-endian ordering convention of the quantum simulator.

2.3 scRNA-seq count matrix generation

The simulation process begins by measuring the final quantum state $|\psi_{\text{final}}\rangle$ multiple times to obtain a histogram of the measurement outcomes. These outcomes are recorded into two distinct classical registers, allowing the probability distribution (marginalized for each cell state) to be assessed separately. This distribution is then used to assess the co-occurrence of gene activation (features) across m observation (simulated single-cells).

A binary count matrix X' is first constructed from this measurement histogram. Each measured bit string, $b = b_0 b_1 \dots b_{n-1}$, corresponds to a single-cell observation where the value $b_i \in \{0, 1\}$ indicates the deactivation or activation (expression) of gene i , respectively. If a bit string b has a measured count of $C(b)$, it contributes $C(b)$ rows to the $n \times m$ matrix X' , where n is the number of genes. The binarization process can be formally represented by defining the matrix element X'_{ij} for gene i in cell j :

$$X'_{ij} = \begin{cases} 1 & \text{if gene } i \text{ is 'ON' in bit string } b_j \\ 0 & \text{if gene } i \text{ is 'OFF' in bit string } b_j \end{cases} \quad (5)$$

The generated binary count matrix X' is then transformed to incorporate the continuous and noisy characteristics of gene expression counts observed in real single-cell data. This is achieved by multiplying the observed 'ON' states ($X'_{ij} = 1$) by a value sampled from the Negative Binomial distribution, a function commonly attributed to the overdispersed count data characteristic of scRNA-seq[11]. The final gene count matrix X is calculated as:

$$X_{ij} = NB(r_i, p_i)X'_{ij}. \quad (6)$$

Here, $NB(r_i, p_i)$ is the Negative Binomial (NB) distribution parameterized by gene-specific parameters, where r_i (often related to dispersion) is the number of successful trials, and p_i is the probability of success. p_i is defined as $p_i = r_i/(\mu_i + r_i)$, where μ

is the i -gene mean. This transformation ensures that the final count X_{ij} remains 0 if the gene was not activated in the quantum measurement ($X'_{ij} = 0$), but if $X'_{ij} = 1$, the expression level follows the stochastic, overdispersed behavior of a real gene. The parameters r_i and p_i are typically designed to mimic real scRNA-seq data to match the marginal statistics of the genes being modeled[8, 12].

2.4 Classical gene regulatory network inference

To benchmark the complexity and non-classical nature of the synthetic data, classical Gene Regulatory Network (GRN) inference methods were applied. Prior to inference, the raw scRNA-seq count matrix X was preprocessed following standard single-cell analysis practices[13, 14]:

1. **Normalization:** Total counts were normalized to 10,000 per cell to correct for sequencing depth differences.
2. **Transformation:** The data was \log_{1p} -transformed to stabilize the variance and mitigate the influence of large count magnitudes[15].
3. **Scaling:** The data was standardized (Z-score scaled) per gene to ensure all features contributed equally to the correlation metrics.

Using this preprocessed matrix, gene-gene correlation matrices were computed across the cells using both the **Pearson** (linear) and **Spearman** (monotonic non-linear) correlation coefficients[16–18]. An adjacency matrix was then constructed by setting a strict threshold, retaining only edges where the absolute correlation value was greater than 0.5 ($|\text{Corr}| > 0.5$). The resulting network topology was visualized using the NetworkX package, allowing for a direct comparison between the programmed quantum entanglement and the inferred classical dependencies[19].

3 Results

Our initial simulation demonstrates the capability of the quantum kernel to model both intra-cellular (GRN) and inter state (cell-cell) regulation. The demonstration utilizes a system composed of five genes ($n = 5$) for Cell Type 1 and five genes ($n' = 5$) for Cell Type 2.

3.1 Parameter initialization and qubit mapping

The initial self-activation level for each gene is set by its corresponding rotation angle θ_i , as defined in Eq. 1. Since the R_y gate maps 0 to the ‘OFF’ state and π to the ‘ON’ state (a full activation), the coefficients $\mathbf{p}_i = \theta_i/\pi$ represent the proportional initial activation of each gene. These values are listed in Table 1.

To establish an unambiguous indexing system, the system’s $n + n' = 10$ qubits are mapped sequentially, following the augmentation in Eq. 3. This creates a **Global Gene Index** g_i (where $i = 0$ to 9) that is identical to the **Qubit Index** q_i . Specifically:

- Genes g_0 to g_4 correspond to **Cell Type 1 (CT1)**.
- Genes g_5 to g_9 correspond to **Cell Type 2 (CT2)**.

We will interchangeably utilize the global index notation $q_i \leftrightarrow g_i$ throughout the remainder of this work.

Table 1 Initial gene activation parameters and qubit mapping

Global Index (q_i/g_i)	Activation $p_i = \theta_i/\pi$	Cell Type	Local Gene Index
$q_0 \equiv g_0$	0.2	CT1	g_0^{CT1}
$q_1 \equiv g_1$	0.1	CT1	g_1^{CT1}
$q_2 \equiv g_2$	0.4	CT1	g_2^{CT1}
$q_3 \equiv g_3$	0.9	CT1	g_3^{CT1}
$q_4 \equiv g_4$	0.8	CT1	g_4^{CT1}
<hr/>			
$q_5 \equiv g_5$	0.2	CT2	g_0^{CT2}
$q_6 \equiv g_6$	0.3	CT2	g_1^{CT2}
$q_7 \equiv g_7$	0.2	CT2	g_2^{CT2}
$q_8 \equiv g_8$	0.7	CT2	g_3^{CT2}
$q_9 \equiv g_9$	0.5	CT2	g_4^{CT2}

3.2 Entanglement and cascade activation

The **entanglement topology** defining both the intra- and inter-state gene regulatory interactions was set using the control-target list L .

3.2.1 Case 1: Inter-state cascade

In the first case, we designed a specific **inter-state cascade** utilizing the entanglement topology $L_1 = \{(3, 5), (5, 7), (7, 0)\}$. This configuration, applied in the $|\psi_{\text{final}}\rangle$ stage (Eq. 4), models a multi-step regulatory path spanning both cell types:

s

- **Step 1 (CT1 \rightarrow CT2):** Gene g_3^{CT1} (qubit q_3) activates gene g_0^{CT2} (qubit q_5).
- **Step 2 (CT2 \rightarrow CT2):** Gene g_0^{CT2} (qubit q_5) activates gene g_2^{CT2} (qubit q_7).
- **Step 3 (CT2 \rightarrow CT1):** Gene g_2^{CT2} (qubit q_7) activates gene g_0^{CT1} (qubit q_0).

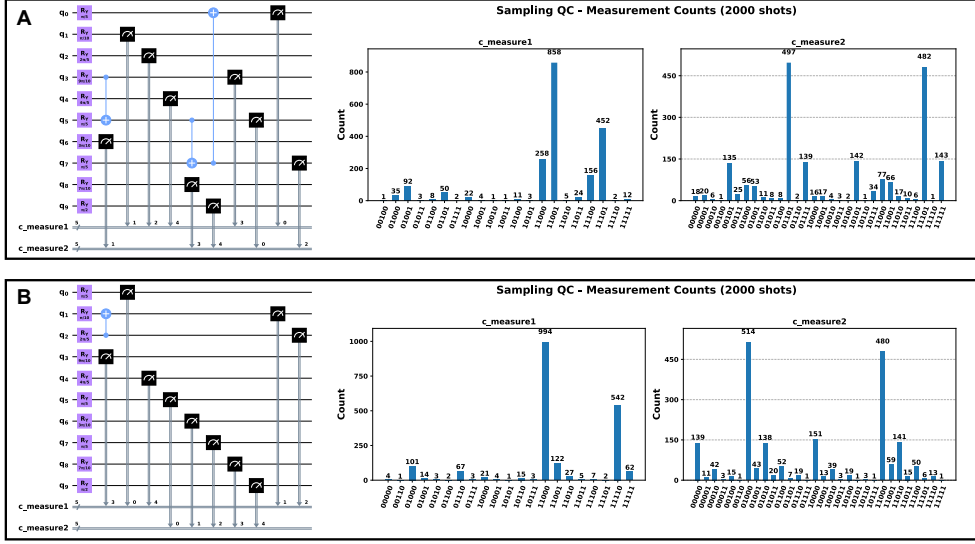
The resulting entangled state $|\psi_{\text{final}}\rangle$ reflects this cascade. The entangling topology and the resulting measurement histogram are shown in Fig. 2A.

3.2.2 Case 2: Non-interacting control

To highlight the effect of the inter-state communication, we performed a control experiment. We used the same activation angles (Table 1) but replaced the complex cascade with a simple, **non-communicating intra-state entangler** $L_2 = \{(2, 1)\}$. This design models an isolated regulation within CT1 (affecting g_2^{CT1} and g_1^{CT1}) and enforces no communication between CT1 and CT2.

Fig. 2B shows the resulting measurement histogram for this non-cascading topology. A visual comparison between the histograms in Fig. 2A and 2B demonstrates

how the programmed entangling topology significantly alters the final co-expression patterns.



3.4 Analysis of entanglement on cell lineage

The synthetic scRNA-seq data, visualized in the UMAP plot in Fig. 3, reveals a clear distinction between the two entanglement scenarios.

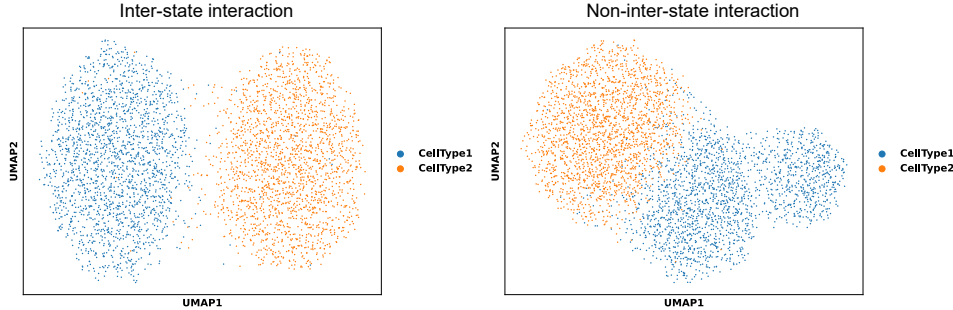


Fig. 3 Simulated scRNA-seq UMAP visualization. The UMAP plot displays the synthetic single-cell data generated under two different entanglement scenarios (Case 1: Inter-state cascade; Case 2: Non-interacting control), showing the resulting lineage separation between CT1 and CT2 populations.

- **Inter-state cascade (case 1):** The data generated with the inter-state regulatory cascade shows a distinct separation of the CT1 and CT2 lineages in Fig. 3. This pronounced separation is due to two factors: the enforced cross-type expression enhancement, and the structural exclusion of gene expression, where CT2 genes (q_5-q_9) have zero expression in CT1 cells and, conversely, CT1 genes (q_0-q_4) have zero expression in CT2 cells[21]. This structural sparsity, combined with entanglement, drives the populations into structurally different high-dimensional states.
- **Non-interacting control (case 2):** Conversely, the non-interacting control experiment (where entanglement was restricted to only $L_2 = \{(2, 1)\}$) exhibits a more mixed or less pronounced separation. In this case, the expression pattern is primarily dominated by the uniformly highly expressed HKGs and the non-interacted model genes. The inter-state cascade is essential for providing the unique, non-linear expression patterns that maximize the separation of the cell states[21].

The observed lineage separation confirms that the quantum entanglement, specifically when programmed to facilitate cross-state regulation, is the dominant factor shaping the distinct expression profiles of CT1 and CT2.

3.5 Synthetic scRNA-seq data analysis and classical predictions

The synthetic scRNA-seq data produced from quantum computing kernel has complex relationships that would be hard to embed from classical regime, but we can still see if from classical regime, we could get the graphs of what was embedded. To this purpose, we propose two analysis, one being the GRN through correlation methods,

e.g. Pearson or Spearman[17, 18]. Where the second is to apply CellChat2.0 to see if we can get the cell communication difference within the two previous cases.

3.5.1 Gene regulatory networks from synthetic data

The classical network inference results, presented in Fig. 4, compare the predicted GRNs against the programmed quantum entanglement topologies. The networks were constructed using a strong absolute correlation threshold of $|\text{Corr}| > 0.5$ on the fully preprocessed (normalized, \log_{1p} -transformed, and scaled) synthetic data.

The analysis reveals that both Pearson and Spearman correlation methods, despite filtering out the background “noise” (HKGs), do not recover the programmed quantum entanglement topology but instead report emergent correlation structures among the model genes[22]. The computed adjacency matrices are highly fragmented and structurally distinct from the CX paths:

Case 1: Inter-state cascade

The programmed quantum cascade was $\mathbf{q}_3 \rightarrow \mathbf{q}_5 \rightarrow \mathbf{q}_7 \rightarrow \mathbf{q}_0$. The classical networks yield connections only among the model genes, successfully excluding the high-magnitude HKGs. However, they report relationships that are emergent effects of the quantum state, not the direct CX links:

- The **Pearson** network (left, Fig. 4A) identifies strong correlations among g_3, g_4, g_5 , and g_7 . The structure forms a single, fragmented component. This high correlation is interpreted as a **coincidental statistical artifact** driven by the differential initial activation, specifically:
 1. The correlation is primarily influenced by the single dominant initial activation angle ($\theta_4 = 0.9\pi$) of gene g_4 . This high base probability of being ‘ON’ creates a statistical tendency to co-occur strongly with its neighbors (g_3, g_5, g_7), regardless of the true quantum causal path.
 2. The network is **structurally incorrect** (e.g., omitting the final target gene, g_0), demonstrating that Pearson’s method prioritizes **emergent statistical co-occurrence** resulting from high base probability over the subtle causal changes introduced by the CX entangling gates.
- The **Spearman** network (right, Fig. 4A) finds a higher density of non-linear monotonic dependencies[22], resulting in a highly interlinked graph involving $g_0, g_3, g_4, g_5, g_7, g_8$. This complex structure does not resemble the targeted regulatory path but confirms that the entanglement creates widespread, complex **non-linear statistical co-dependencies** among the model genes.

Case 2: Non-interacting control

The simple programmed link was $\mathbf{q}_2 \rightarrow \mathbf{q}_1$. The networks are sparse and report almost no meaningful inter-gene connections. The initial conditions for the programmed genes are $\theta_2 = 0.4\pi$ and $\theta_1 = 0.1\pi$, while the strongest self-activations are on g_3 ($\theta_3 = 0.9\pi$), g_4 ($\theta_4 = 0.8\pi$) and g_8 ($\theta_8 = 0.7\pi$):

- The **Pearson** network (left, Fig. 4B) is minimal, identifying two isolated pairs: $g_1 - g_2$ and $g_3 - g_4$, with g_8 also present as an isolated node. Crucially, the programmed link $\mathbf{q}_2 \rightarrow \mathbf{q}_1$ (the $g_2 \rightarrow g_1$ connection) is **recovered** as a strong correlation between g_1 and g_2 . However, the strong $g_3 - g_4$ link represents a spurious correlation driven by the high base activation of those genes.
- The **Spearman** network (right, Fig. 4B) finds a similarly sparse and highly fragmented structure[22]. While it **recovers the $g_1 - g_2$ connection**, the remaining links are likely **coincidental correlations** driven by the differential self-activation angles (θ_i) rather than genuine entanglement effects. For instance, the genes g_3 and g_4 form an isolated pair, and g_8 remains an isolated node, confirming that the majority of connections are artifacts stemming from the initial high-probability states.

Interpretation: Quantum causality vs. classical correlation

The analysis confirms a critical distinction between the programmed quantum causality and the emergent classical correlations. The consistent finding is that the classical methods successfully filtered out the background noise (HKGs) but only captured **partially correct interactions** and failed to reconstruct the complete programmed CX paths.

The quantum kernel establishes **causal dependencies** ($CX_{i,j}$) which, through superposition and measurement, result in a **complex joint probability distribution**. The final classical correlations are not the direct causal links, but rather **emergent statistical relationships** created by the entanglement on the sampled state.

- **High-probability bias:** The Pearson method, in the inter-state cascade (case 1), was heavily influenced by the single dominant initial activation angle ($\theta_4 = 0.9\pi$) of g_4 . This led to coincidental statistical artifacts—structurally incorrect correlations ($g_3 - g_4$)—that overshadowed the true quantum links, demonstrating the method's vulnerability to high base probability over subtle quantum signals.
- **Incomplete recovery:** While the simple programmed link ($\mathbf{q}_2 \rightarrow \mathbf{q}_1$) was successfully recovered in the non-interacting control (case 2), the presence of other connections (e.g., $g_3 - g_4$) are artifacts of the non-interacting genes' **high base activation angles** (θ_i). This confirms that the methods are easily biased by varying initial probabilities, resulting in misleading correlation structures.

This demonstrates that the quantum-generated data does not represent a simple sum of linear or monotonic pairwise relationships, but rather exhibits **non-classical dependencies** that fundamentally challenge standard correlation-based classical analysis tools, even when rigorous preprocessing is applied[23].

3.5.2 Cell-cell communication inference from synthetic data

We applied CellChat2.0 to our synthetic scRNA-seq data to evaluate the impact of our embedded regulatory mechanisms, leveraging the tool's capability to infer cell-cell communication by modeling the projected interaction probability for Ligand-Receptor (LR) [24]. Our core objective was to determine if a customized LR database, in junction

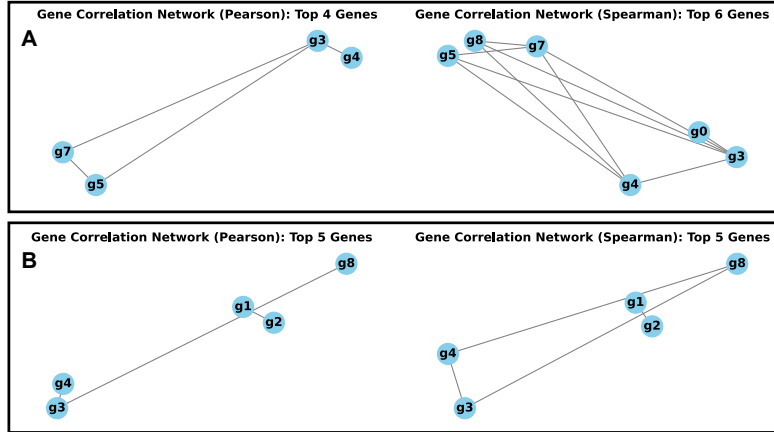


Fig. 4 Gene regulatory networks through classical prediction. A) shows GRN inference through Pearson and Spearman correlation computed adjacency matrix above 0.5 threshold for inter-state interaction simulation. B) shows GRN inference through Pearson and Spearman correlation computed adjacency matrix above 0.5 threshold for non-inter-state simulation.

with CellChat2.0, could accurately distinguish between true mechanistic interactions embedded in the data and false, coincidental correlations arising from other highly expressed genes (entanglements).

Our designed setup included two sets of LR pairs in the custom database: the true inter-state interactions ($g_3 \rightarrow g_5$ and $g_7 \rightarrow g_0$), which are mechanistically responsible for the cell-cell communication, and false control pairs ($g_8 \rightarrow g_4$ and $g_9 \rightarrow g_4$), which were included to test the prediction of coincidental probability. These four simulated LR interactions are detailed in Table 2.

Table 2 Simulated Ligand-Receptor interactions

Interaction Name	Pathway	Ligand	Receptor	Annotation	Evidence
g3-g5_simulated	Simulated1	g3	g5	Secreted Signaling	Simulated1
g7-g0_simulated	Simulated2	g7	g0	Secreted Signaling	Simulated2
g8-g4_simulated	Simulated3	g8	g4	Secreted Signaling	Simulated3
g9-g4_simulated	Simulated4	g9	g4	Secreted Signaling	Simulated4

The results presented in Table 3, validate that our proposed gene activations (from Table 1) and the corresponding entanglement topologies (L_1 and L_2) provide strong mechanistic insights. As expected, the true LR pairs demonstrated a robust increase in communication probability when the inter-state interaction was active. For instance, the LR pair $g_3 \rightarrow g_5$ saw its probability from 0.0148 (non-interacting) to 0.1135 (inter-state interaction), a boost of over 7-fold. The LR pair $g_7 \rightarrow g_0$ exhibited an even more dramatic increase, becoming approximately 75 times more likely to occur. These findings are consistent with our design, where the entanglement was aligned by the master gene regulator, g_3 .

Conversely, the false LR pairs, which were included in the database but corresponded only to coincidentally highly active genes, were minimally affected. This outcome was anticipated, as no direct entanglement (mechanistic link) was set for these scenarios. For instance, the communication probability for $g_9 \rightarrow g_4$ showed only a marginal change, shifting from 0.0726 in the non-interacting state to 0.0638 in the interacting state, resulting in a ratio of 0.88 (nearly 1). This demonstrates that the inference method successfully distinguished true mechanistic links from simple co-activation based purely on gene expression [25]. Crucially, while the method still assigned a confident probability link (and $p\text{-val}=0$) even when no mechanistic interaction was present, this high confidence can be misleading[26]. It is critical to note that the absolute probability value alone suggests a link exists when not compared; thus, the relative change in probability between the two conditions—not the absolute p -value—proved to be the key metric for reliably validating the synthetic mechanistic links[27].

Table 3 CellChat Ligand-Receptor Inference with Simulated Pairs

Source	Target	Ligand	Receptor	Prob.	p-val	Pathway	Dataset
CT1	CT2	g3	g5	0.0148	0	Simulated1	Non-interacting
CT2	CT1	g7	g0	0.0011	0	Simulated2	Non-interacting
CT2	CT1	g8	g4	0.1133	0	Simulated3	Non-interacting
CT2	CT1	g9	g4	0.0726	0	Simulated4	Non-interacting
CT1	CT2	g3	g5	0.1135	0	Simulated1	Inter-state interaction
CT2	CT1	g7	g0	0.0830	0	Simulated2	Inter-state interaction
CT2	CT1	g8	g4	0.1008	0	Simulated3	Inter-state interaction
CT2	CT1	g9	g4	0.0638	0	Simulated4	Inter-state interaction

4 Discussion and conclusions

Our work introduces a novel hybrid quantum-classical simulator, qSimCells, that addresses fundamental limitations in classical scRNA-seq data simulation[12] by leveraging quantum entanglement to encode complex, nonlinear gene regulatory network (GRN) and cell-cell communication (CCC) topologies. The key advantage of the quantum kernel is its ability to enforce causal dependencies through the time-ordered application of CX gates[9], establishing an explicit directionality, a true cause-and-effect link, such as the programmed cascade $g_3 \rightarrow g_5 \rightarrow g_7 \rightarrow g_0$, that is impossible to encode directly in classical correlation-based simulators[12]. The results demonstrate that the synthetic data possesses non-classical dependencies, making it an ideal ground truth for benchmarking advanced methods and highlighting the inherent weaknesses of traditional classical inference techniques.

The comparative analysis demonstrates the critical limitations of standard classical network inference (GRN) methods, such as Pearson and Spearman correlation[17],

[18, 28], when applied to this quantum-generated data. Both methods failed to reconstruct the complete programmed CX paths, instead reporting emergent statistical artifacts—relationships created by the overall complex probability distribution rather than the discrete, causal CX links (Fig. 4). Classical networks were highly vulnerable to the high base probability set by the initial gene activation angles (θ_i), leading to spurious correlations (e.g., $g_3 - g_4$) that overshadowed the subtle signals introduced by the quantum entanglement[12]. This confirms that classical correlation methods prioritize the magnitude of gene expression over the subtle, nonlinear quantum causal changes and are fundamentally limited by their symmetric nature, failing to recover the true directionality embedded by the quantum kernel.

The application of CellChat2.0 to the inter-state communication provided a strong validation of our quantum ground truth while simultaneously exposing a critical methodological weakness in general cell-cell communication inference[29]. On one hand, the tool successfully validated the true LR pairs ($g_3 \rightarrow g_5$ and $g_7 \rightarrow g_0$) by showing a robust increase in communication probability (~ 7 to 75-fold) when the true signal was present. On the other hand, the false LR pairs, which had no programmed entanglement, were still assigned a high confidence probability (e.g., $p\text{-val}=0$). This high absolute confidence, even in the absence of a mechanistic link, is highly misleading if not compared across conditions. Therefore, our work concludes that for rigorous mechanistic validation in real-world data, the relative change in probability between two distinct conditions (e.g., interacting vs. non-interacting) is the key metric required to distinguish true causal signaling from spurious correlations arising from high gene co-expression[30].

In conclusion, our hybrid quantum-classical simulator provides a superior platform for generating synthetic scRNA-seq data[31]. By utilizing quantum entanglement, we create a high-fidelity ground truth of causal interactions (with inherent directionality and non-linearity) that fundamentally challenges and thereby improves the testing capabilities for current computational tools[32, 33]. This work confirms that the quantum kernel is essential for creating data where the ground truth is unequivocally known, highlighting the need for advanced inference techniques that can move beyond simple linear correlations to capture the complex, non-classical dependencies inherent in gene regulation[34].

Supplementary information

If your article has accompanying supplementary file/s please state so here.

Acknowledgements

Declarations

- **Funding:** This study was funded by the U.S. Department of Defense (DoD, GW200026) and the National Institute for Environmental Health Sciences (P30 ES029067) for J.J.C, Allen Endowed Chair in Nutrition & Chronic Disease Prevention for R.S.C., and the Cancer Prevention & Research Institute of Texas (CPRIT,

RP230204) for J.J.C. and R.S.C.

- **Conflict of interest:** The authors have no conflict of interest.
- **Data availability:** Our algorithm is publicly available on GitHub <https://github.com/cailab-tamu/qSimCells>.
- **Author contribution:** Authors...

Appendix A Section title of first appendix

An appendix contains supplementary information that is not an essential part of the text itself but which may be helpful in providing a more comprehensive understanding of the research problem or it is information that is too cumbersome to be included in the body of the paper.

References

- [1] Hwang, B., Lee, J.H., Bang, D.: Single-cell rna sequencing technologies and bioinformatics pipelines. *Experimental & molecular medicine* **50**(8), 1–14 (2018)
- [2] Huynh-Thu, V.A., Sanguinetti, G.: Gene regulatory network inference: an introductory survey. In: *Gene Regulatory Networks: Methods and Protocols*, pp. 1–23. Springer, ??? (2018)
- [3] Dibaeinia, P., Sinha, S.: Sergio: a single-cell expression simulator guided by gene regulatory networks. *Cell systems* **11**(3), 252–271 (2020)
- [4] Li, H., Zhang, Z., Squires, M., Chen, X., Zhang, X.: scmultisim: simulation of multi-modality single cell data guided by cell-cell interactions and gene regulatory networks. *Research Square*, 3 (2023)
- [5] Herbach, U.: Harissa: stochastic simulation and inference of gene regulatory networks based on transcriptional bursting. In: *International Conference on Computational Methods in Systems Biology*, pp. 97–105 (2023). Springer
- [6] Xiao, F., Tang, J., Fang, H., Xi, R.: Gene regulatory network in single cells based on the poisson log-normal model. *arXiv preprint arXiv:2111.04037* (2021)
- [7] Roman-Vicharra, C., Cai, J.J.: Quantum gene regulatory networks. *npj Quantum Information* **9**(1), 67 (2023)
- [8] Zappia, L., Phipson, B., Oshlack, A.: Splatter: simulation of single-cell rna sequencing data. *Genome biology* **18**(1), 174 (2017)
- [9] Nielsen, M.A., Chuang, I.L.: *Quantum Computation and Quantum Information*. Cambridge university press, ??? (2010)

- [10] Aleksandrowicz, G., et al.: Qiskit: An open-source framework for quantum computing (2019) <https://doi.org/10.5281/zenodo.2562111>
- [11] Dadaneh, S.Z., Figueiredo, P., Sze, S.-H., Zhou, M., Qian, X.: Bayesian gamma-negative binomial modeling of single-cell rna sequencing data. *BMC genomics* **21**(Suppl 9), 585 (2020)
- [12] Crowell, H.L., Morillo Leonardo, S.X., Soneson, C., Robinson, M.D.: The shaky foundations of simulating single-cell rna sequencing data. *Genome Biology* **24**(1), 62 (2023)
- [13] Butler, A., Hoffman, P., Smibert, P., Papalexi, E., Satija, R.: Integrating single-cell transcriptomic data across different conditions, technologies, and species. *Nature biotechnology* **36**(5), 411–420 (2018)
- [14] Luecken, M.D., Theis, F.J.: Current best practices in single-cell rna-seq analysis: a tutorial. *Molecular systems biology* **15**(6), 8746 (2019)
- [15] Bacher, R., Kendziora, C.: Design and computational analysis of single-cell rna-sequencing experiments. *Genome biology* **17**(1), 63 (2016)
- [16] Faith, J.J., Hayete, B., Thaden, J.T., Mogno, I., Wierzbowski, J., Cottarel, G., Kasif, S., Collins, J.J., Gardner, T.S.: Large-scale mapping and validation of escherichia coli transcriptional regulation from a compendium of expression profiles. *PLoS biology* **5**(1), 8 (2007)
- [17] Pearson, K.: VII. note on regression and inheritance in the case of two parents. *proceedings of the royal society of London* **58**(347-352), 240–242 (1895)
- [18] Spearman, C.: The proof and measurement of association between two things. *The American journal of psychology* **100**(3/4), 441–471 (1987)
- [19] Hagberg, A., Swart, P.J., Schult, D.A.: Exploring network structure, dynamics, and function using networkx. Technical report, Los Alamos National Laboratory (LANL), Los Alamos, NM (United States) (2008)
- [20] Houkpe, B.W., Chenou, F., De Lima, F., De Paula, E.V.: Hrt atlas v1. 0 database: redefining human and mouse housekeeping genes and candidate reference transcripts by mining massive rna-seq datasets. *Nucleic acids research* **49**(D1), 947–955 (2021)
- [21] Zhang, S., Pyne, S., Pietrzak, S., Halberg, S., McCalla, S.G., Siahpirani, A.F., Sridharan, R., Roy, S.: Inference of cell type-specific gene regulatory networks on cell lineages from single cell omic datasets. *Nature Communications* **14**(1), 3064 (2023)
- [22] Wang, Y., Li, Y., Cao, H., Xiong, M., Shugart, Y.Y., Jin, L.: Efficient test for

nonlinear dependence of two continuous variables. *BMC bioinformatics* **16**(1), 260 (2015)

- [23] González-Guillén, C.E., Lancien, C., Palazuelos, C., Villanueva, I.: Random quantum correlations are generically non-classical. In: *Annales Henri Poincaré*, vol. 18, pp. 3793–3813 (2017). Springer
- [24] Jin, S., Guerrero-Juarez, C.F., Zhang, L., Chang, I., Ramos, R., Kuan, C.-H., Myung, P., Plikus, M.V., Nie, Q.: Inference and analysis of cell-cell communication using cellchat. *Nature communications* **12**(1), 1088 (2021)
- [25] Dimitrov, D., Türei, D., Garrido-Rodriguez, M., Burmedi, P.L., Nagai, J.S., Boys, C., Ramirez Flores, R.O., Kim, H., Szalai, B., Costa, I.G., *et al.*: Comparison of methods and resources for cell-cell communication inference from single-cell rna-seq data. *Nature communications* **13**(1), 3224 (2022)
- [26] Benjamini, Y., Hochberg, Y.: Controlling the false discovery rate: a practical and powerful approach to multiple testing. *Journal of the Royal statistical society: series B (Methodological)* **57**(1), 289–300 (1995)
- [27] Storey, J.D.: A direct approach to false discovery rates. *Journal of the Royal Statistical Society Series B: Statistical Methodology* **64**(3), 479–498 (2002)
- [28] Ali, S.I.M., Alrashid, S.Z.: A review of methods for gene regulatory networks reconstruction and analysis: Sim ali, sz alrashid. *Artificial Intelligence Review* **58**(8), 256 (2025)
- [29] Jin, S., Plikus, M.V., Nie, Q.: Cellchat for systematic analysis of cell-cell communication from single-cell transcriptomics. *Nature protocols* **20**(1), 180–219 (2025)
- [30] Pratapa, A., Jalihal, A.P., Law, J.N., Bharadwaj, A., Murali, T.: Benchmarking algorithms for gene regulatory network inference from single-cell transcriptomic data. *Nature methods* **17**(2), 147–154 (2020)
- [31] Cao, Y., Yang, P., Yang, J.Y.H.: A benchmark study of simulation methods for single-cell rna sequencing data. *Nature communications* **12**(1), 6911 (2021)
- [32] Lasri, A., Shahrezaei, V., Sturrock, M.: Benchmarking imputation methods for network inference using a novel method of synthetic scRNA-seq data generation. *BMC bioinformatics* **23**(1), 236 (2022)
- [33] Kubacki, M., Niranjan, M.: Quantum annealing-based clustering of single cell rna-seq data. *Briefings in Bioinformatics* **24**(6), 377 (2023)
- [34] Zhang, S., Pyne, S., Pietrzak, S., Halberg, S., McCalla, S.G., Siahipirani, A.F., Sridharan, R., Roy, S.: Inference of cell type-specific gene regulatory networks on

cell lineages from single cell omic datasets. *Nature Communications* **14**(1), 3064 (2023)